SASEC2015
Third Southern African Solar Energy Conference
11 – 13 May 2015
Kruger National Park, South Africa

Computational Investigation of Worst-Case Wind Loads on a Heliostat Pod for Different Reflector Aspect Ratios

Marais M.D., Craig K.J.* and Meyer J.P.
*Author for correspondence
Department of Mechanical and Aeronautical Engineering,
University of Pretoria,
Pretoria, 0002,
South Africa,
E-mail: ken.craig@up.ac.za

ABSTRACT

Heliostat structures contribute significantly to the cost of a central receiver power plant. This study was concerned with obtaining wind loadings on a modular heliostat pod (HelioPOD) that houses six reflectors as developed by Stellenbosch University's Solar Thermal Research Group (STERG) using computational fluid dynamics (CFD). Mean wind loadings were obtained for different combinations of elevation and azimuth angle, as well as different reflector aspect ratios, meshing and parameterizing the domain with *ANSYS Workbench v15.0* and solving the steady-state flow field using *ANSYS Fluent.*

INTRODUCTION

Heliostat structures make up 40% to 50% of the initial capital cost of a central receiver power plant [1]. For this reason there is a substantial amount of research directed towards designing more cost-effective heliostat arrangements. Figure 1 shows the HelioPOD structure developed by STERG to simplify installation and centralize control. The numbering convention used to identify the heliostats in this paper is also shown. The design is constantly evolving, but at time of writing had a reflector aspect ratio of $r_a = b/h = 1.5$ and a reflector area of $A_{ref} = 2.23$ m^2. The reflector centre is 1.38 m above ground level and is offset from the pylon (pylon height above ground is 1.17 m) by the drives and mounting mechanism.

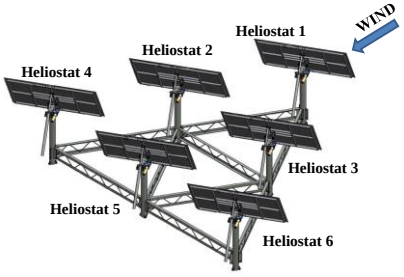

Figure 1: HelioPOD arrangement with six reflectors

A heliostat structure located in an open country environment will be subjected to an attacking atmospheric wind with velocity and turbulence intensity profiles characteristic of the terrain roughness. Such profiles have to be adequately modeled to ensure that they resemble the terrain where the site is to be located and that the turbulence does not dissipate before reaching the heliostat model. Experimental [2,3] and numerical [4,5] studies have been performed for isolated heliostat structures but a more thorough investigation of how the flow field interacts with six reflectors on a pod is needed for adequate structural design. The deliverables of this study were wind loading forces and moments to allow for structural design and optimization to be performed.

The minimum requirements relevant to wind loadings and appropriate design of the heliostat structure are listed in Table 1 as they were presented by STERG during SASEC 2014 [6].

Table 1: Relevant heliostat requirements [6]

Requirement	Minimum Requirement Value
On-target accuracy	1.875 mrad normal vector error 150 mm deviation (target at a 40 m slant range)
Component accuracy	0.625 mrad RMS tracking error 0.625 mrad pedestal flex 0.625 mrad mechanism flex
Operational winds	**Track up to 20 km/h** **Stow between 20 km/h and 50 km/h**
Survival winds	Survive stow loads of up to 100 km/h

From Table 1 we may obtain an indication of what the wind speed should be for the CFD investigation to ensure the final design meets the remaining requirements. A heliostat moving into stow position can be orientated in many ways with reference to an attacking atmospheric wind, therefore it was decided to use the upper limit of the stow wind speed as the reference value: $u_{ref} = 15$ m/s (54 km/h) was chosen at a reference height of $z_{ref} = 1.38$ m, which is the height above ground of the reflector center.

If a log-law velocity profile like that in Equation 1 is assumed with an aerodynamic roughness length of $z_0 = 0.03$ m for open terrain, then the velocity at 10 m above ground equates to 22.8 m/s. The chosen wind speed is therefore in line with the requirements as laid out by Strachan and Houser [7] and later reiterated by Roos [8]: A heliostat must be able to operate, without static failure or low-cycle fatigue, in any position in a 22 m/s wind as measured 10 m above ground level.

$$u(z) = u_{ref}\frac{\ln(z/z_0)}{\ln(z_{ref}/z_0)} \quad (1)$$

The coordinate system used for this study is shown in Figure 2. It differs from that used in a previous study [4] in that it does not rotate with the heliostat about the *z*-axis, instead the local coordinate system at each pylon is aligned with the global directions which allows the force and moment components caused by wind loadings on the reflector to be expressed. The orientations angles are such that $\alpha = 90°, \beta = 0°$ resembles an upright reflector with the wind approaching it head on.

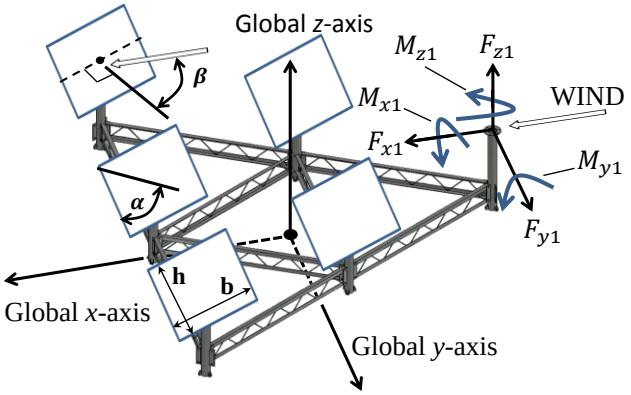

Figure 2: Coordinate system, reference lengths and orientation angles

Three main CFD investigations were conducted during this study and are summarised in Table 2. In short, these may be described as 1) a model-scale domain that replicated the geometry of the 1/60th scale heliostat tested by Peterka, *et al.* [2] for validation, 2) a similar domain as the first, but scaled to full size and with the single heliostat replaced by a HelioPOD with six reflectors and six pylons and 3) another full-scale domain but with periodic boundary conditions on the side walls to study the effect of a continuous heliostat field.

Table 2: Summary of the CFD investigations conducted

	Investigation 1	**Investigation 2**	**Investigation 3**
Aim	Force and moment coefficient at different orientations to validate the CFD approach against the work of Peterka, *et al.* [2]	Forces plus moments at different orientations and aspect ratios considering a standalone HelioPOD	Forces, moments, orientations and aspect ratios. Modelling a HelioPOD that repeats infinitely in both directions
Inlet profiles	1/60th scale: u ($z_0 = 0.5$ mm), k, ε	Full scale: u ($z_0 = 0.03$ m), k and ε	Full scale: u ($z_0 = 0.03$ m), k and ε
Outlet	0 Pa gauge	0 Pa gauge	0 Pa gauge
Top BC	Slip wall	Slip wall	Slip wall
Side BC	Slip wall	Slip wall	Translationally Periodic
Bottom BC	Sandgrain roughness	Sandgrain roughness	Sandgrain roughness
Domain size [x y z]	[3.5 1.3 0.8]	[50 40 15]	[50 2.5 15]
No. of cells	13.3 million	12.2 million	16.5 million
Heliostat	Single model	HelioPOD (See Figure 4)	Periodic repeat (See Figure 5)
Support structure	Pylon, torque tube	Pylons	Pylons, lattice girders
Orientation considered [α β]°	[90 0]° [30 0]° [90 67.5]° [30 180]°	[90 0]° [30 0]° [90 67.5]° [30 180]°	[90 0]° [30 0]° [90 67.5]° [30 180]°
Aspect ratios	$r_a = b/h = 1$	$r_a = 0.\dot{6}; 1; 1.5$	$r_a = 0.\dot{6}; 1; 1.5$
No. of runs	4	12	12

NOMENCLATURE

A_{ref}	[m^2]	Reflector area
b	[m]	Reflector width
C_F	[-]	Force coefficient
C_M	[-]	Moment coefficient
C_{MH}	[-]	Hinge moment coefficient
C_s	[-]	Roughness constant
C_μ	[-]	Turbulence model constant
$E_{\%}$	[%]	Normalised error
F	[N]	Wind induced force
h	[m]	Reflector height
I_u	[%]	Streamwise turbulence intensity
k	[m^2/s^2]	Turbulent kinetic energy
M	[Nm]	Wind induced moment
r_a	[-]	Reflector aspect ratio ($r_a = b/h$)
u	[m/s]	Stream-wise velocity component
x, y, z	[m]	Cartesian coordinates

Special characters

α	[°]	Elevation angle of reflector
β	[°]	Wind angle
ε	[m^2/s^3]	Turbulence dissipation rate
$\kappa_{k\text{-}\varepsilon}$	[-]	Von Karman constant

Subscripts

0	Aerodynamic roughness length
1-6	Indication of the row or individual heliostat considered
ref	Reference value
s	Equivalent sandgrain roughness
x, y, z	In the direction of *x*, *y* or *z*

Superscripts

*	Friction velocity
‘	Fluctuating component

Abbreviations

ABL	Atmospheric boundary layer
BC	Boundary condition
CFD	Computational fluid dynamics
RANS	Reynolds Averaged Navier Stokes

NUMERICAL METHOD

Computational domain and boundary conditions

Operating conditions were at the default *ANSYS Fluent* values with pressure at 101 kPa, the density of air at 1.225 kg/m^3 and the viscosity at 1.7894e^{-5} kg/ms. Air was assumed to be an incompressible, isothermal gas.

In addition to specifying the velocity profile, profiles of turbulent kinetic energy k and turbulence dissipation rate ε were specified according to Equation 2. The profiles were imposed at the inlet by writing a user-defined function, interpreting the code in *ANSYS Fluent* and hooking the profiles to the inlet.

$$k = \frac{u^{*2}_{ABL}}{\sqrt{C_\mu}}; \quad \varepsilon(z) = \frac{u^{*3}_{ABL}}{\kappa_{k-\varepsilon} z} \tag{2}$$

Previous work in wind tunnels provided profiles of velocity and turbulence intensity [2,3]. The assumption of isotropic turbulence and the definition of k allows a relation for I_u to be developed that we can use to compare inlet profiles with what is available in the literature (See Equation 3).

$$I_u(z) = \frac{\sqrt{\overline{u'^2}}}{u(z)} \times 100\% = \frac{\sqrt{\frac{2}{3}k}}{u(z)} \times 100\% \tag{3}$$

In Figure 3 the profiles for $u(z)$ and $I_u(z)$ obtained using Equations 1 and 3 are compared to those of Peterka, *et al.* [2]. The profiles agree relatively well with the experimental values, except that the velocity is under-predicted near the ground.

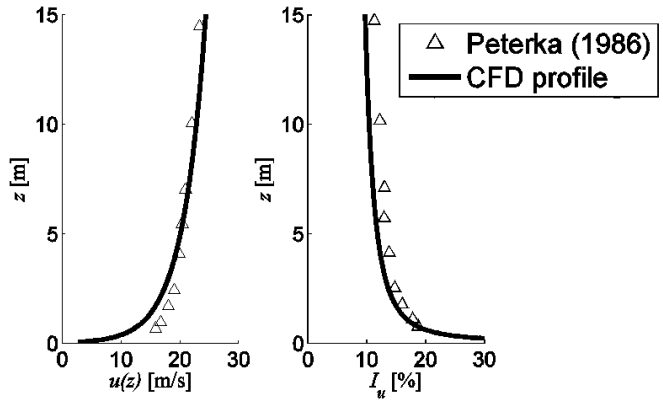

Figure 3: Velocity and turbulence intensity profiles specified at the inlet of the full-scale domain using $z_0 = 0.03$ m

Since the profiles of velocity and turbulence properties are based on an aerodynamic roughness length z_0, it is important to specify a roughness for the bottom of the domain. Specifying an equivalent sandgrain roughness ($z_{s,ABL}$) in *ANSYS Fluent* has been shown to reduce the effects of horizontal inhomogeneity [4] of the ABL and can be achieved by using $z_{s,ABL} = 9.793 z_0 / C_s$ where C_s is a constant with a default value of 0.5 [9].

Two distinct geometries were used for the full-scale simulations. The standalone HelioPOD geometry was simplified to include only the six reflectors and pylons and is shown in Figure 4. The standalone geometry required the computational domain to be extended far to the left and right to mitigate the effect of the domain walls on the solution. By considering a periodically repeating section of the geometry (Figure 5), the computational domain is not as wide (see the domain size in Table 2) and the saving in cells was used to also add and mesh the lattice girders forming the lower part of the support structure.

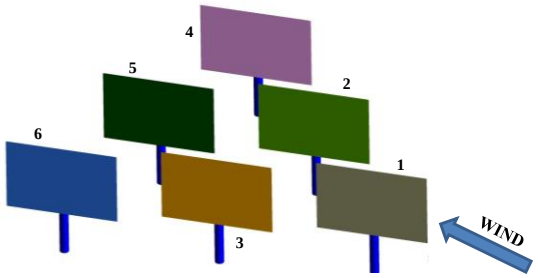

Figure 4: Standalone HelioPOD simplified for CFD simulations

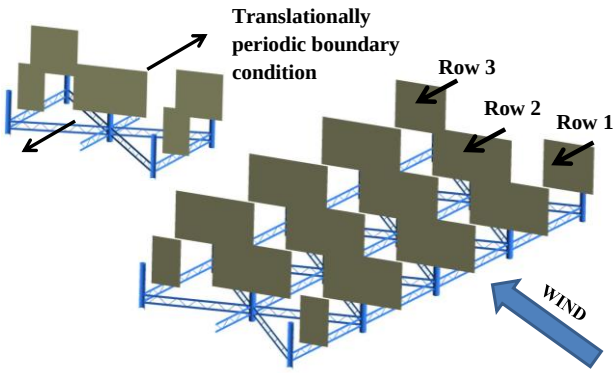

Figure 5: Periodically repeating geometry.

Solver setup

The governing equations were solved using the Coupled solver in *ANSYS Fluent* v15.0. All variables were discretised using second-order methods and convergence was monitored using scaled residuals, monitoring force and moment coefficients and checking for mass balance between inlet and outlet. Turbulence closure was obtained by using the RNG k-ε turbulence model with standard wall functions.

Validation of numerical model (Investigation 1)

In order to validate the CFD method, a numerical model that resembles the experimental study done by Peterka, *et al*. [2] was set up to allow results to be compared. The experiment consisted of a single 1/60th scale heliostat model that was tested in an atmospheric wind tunnel.

After ensuring mesh independence of the aerodynamic coefficients, results were compared to those obtained in the experiment. A normalized error $E_{\%}$ was calculated by dividing the difference between experimental and numerical values by the experimental value. The comparison is shown in Table 3.

The coefficients are mostly under-predicted and a possible reason for this could be the under-prediction of the velocity near ground level (Figure 3). Some coefficients were only given to two decimal places in the original report, often providing only one significant digit to compare results with. In order to compare results to within at least three significant digits, the method suggested by Roos [8] was used to improve resolution of the experimental data to three significant digits.

Table 3: Comparison of validation case to experimental data

α [°]	β [°]	Coefficient	Experimental	CFD	$E_{\%}$ [%]
90	0	C_{Fx}	1.26	1.1308	-10.3
30	0	C_{Fz}	0.798	0.6239	-21.8
90	67.5	C_{Mz}	0.0813	0.0908	11.7
30	180	C_{MHy}	0.155	0.1339	-13.6

Grid size and sensitivity (conducted during Investigation 2)

A CFD solution should ideally be entirely mesh independent and therefore it is good practice to conduct a grid sensitivity study to observe the influence of grid refinement on the results. Four grids of increasing refinement were considered. To limit the extent of the study, a fixed orientation was chosen at which several wind-loading coefficients have significant magnitudes (α = 30°, β = 180°). The refinement consisted of increasing the amount of tetrahedral cells on the surfaces of both the reflector and pylon, as well as decreasing the size of the structured hexagonal cells surrounding the heliostat zone. The former had the effect of more accurately representing the high gradients associated with flow separation from a bluff body whilst the latter improved resolution of the velocity profile near the ground plane.

Table 4: % Difference between consecutive force and moment coefficients during grid refinement for α = 30° and β = 180°

Cells	C_{MHy1}	C_{z1}	C_{MHy5}	C_{z5}
1.98E+06	-	-	-	-
5.37E+06	6.30%	4.16%	2.37%	1.31%
1.22E+07	3.04%	1.91%	0.61%	0.42%
1.77E+07	0.84%	0.60%	0.62%	0.41%

From Table 4 it follows that subsequent grid refinements caused changes in the wind loading coefficients. The finest grid with an excess of 17 million cells still indicates a change in the results, but taking into consideration computational and time resources it was deemed sufficient to conduct this study with a grid consisting of around 12.2 million cells.

CFD RESULTS

Standalone HelioPOD (Investigation 2)

Figure 6 shows a velocity contour plot on a plane located at reflector centre height (z = 1.38 m) as well as a plot of static gauge pressure on the reflectors of a standalone HelioPOD. The shown orientation produced both the highest force (Figure 7) and moment magnitude (Figure 11) among the orientations considered. It should be noted that due to the maximum value of the stow velocity range being chosen for this study, the wind forces and moments are substantially higher than those calculated previously [6]. In that study 20 km/h was used as the reference velocity and peak-loading coefficients were used as opposed to the mean loading values of the current RANS study. Care must therefore be taken during the design of the structure to make sure what the operational envelope will be in terms of velocities and orientation angles.

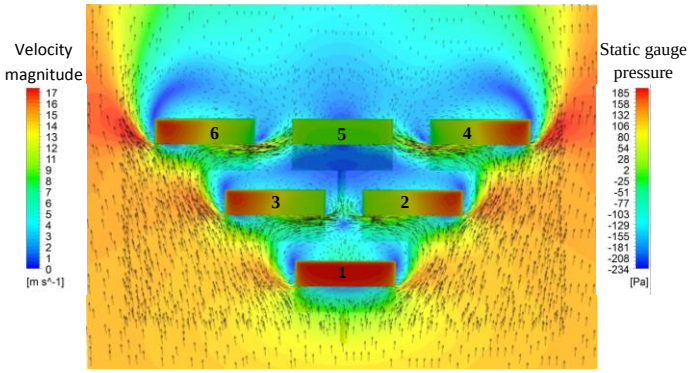

Figure 6: Velocity magnitude (horizontal plane at centre height) and static gauge pressure (reflectors) plots for a standalone HelioPOD ($\alpha = 90°, \beta = 0°$)

Figure 7 to Figure 12 gives values for the forces and moments acting on the pylons as obtained from the CFD simulations. The result for each orientation is given so that the different load cases may be visualised and compared.

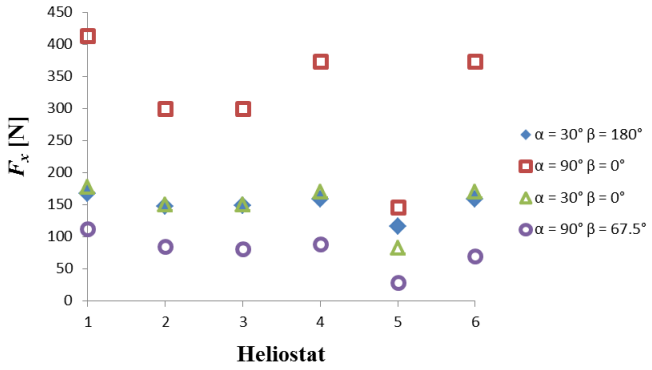

Figure 7: F_x plotted for each heliostat and orientation ($r_a = 1.5$)

From Figure 7 it is observed that the maximum force occurs on the first heliostat (Figure 1) when facing the wind directly. Heliostats located further back experience slightly lower forces, especially heliostat 5 which is the only reflector being completely blocked by surrounding heliostats. Heliostat 1 also experiences the highest lift force (Figure 9) and moment about the x-axis (Figure 10). In Figure 8 a side force is observed (In the y-direction) when the reflectors are upright and rotated about the z-axis.

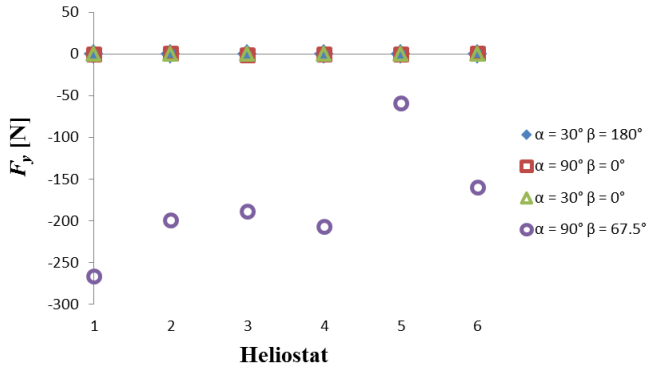

Figure 8: F_y plotted for each heliostat and orientation ($r_a = 1.5$)

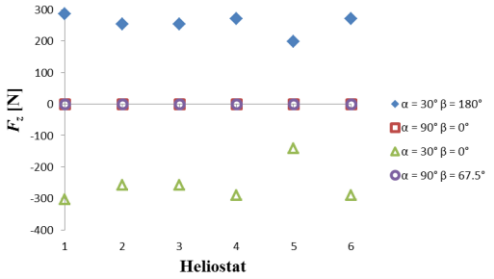

Figure 9: F_z plotted for each heliostat and orientation ($r_a = 1.5$)

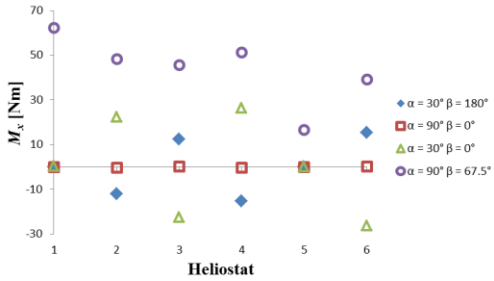

Figure 10: M_x plotted for each heliostat and orientation ($r_a = 1.5$)

In Figure 11 the maximum value of M_y is seen to occur for the first heliostat when in an upright orientation. The maximum M_y for a single heliostat was seen to occur at $\alpha = 30°$, $\beta = 180°$ (See Table 3). The reason for this twofold: 1) in the current design the reflector is offset from the pylon and hence the point where the moment is calculated that makes for a longer moment arm, and 2) due to the logarithmic shape of the velocity profile, a heliostat closer to the ground such as the current design encounters a larger difference between the velocity at the top of the reflector and that at the bottom than would a design that stands taller. There is therefore a larger difference in static pressure between the top and bottom of the reflector, making for a larger M_y.

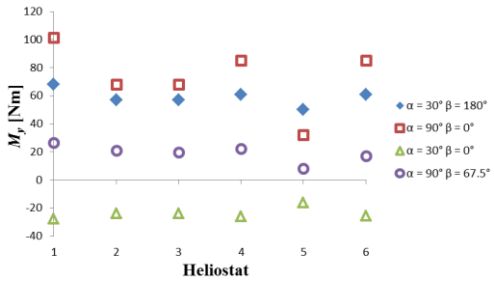

Figure 11: M_y plotted for each heliostat and orientation ($r_a = 1.5$)

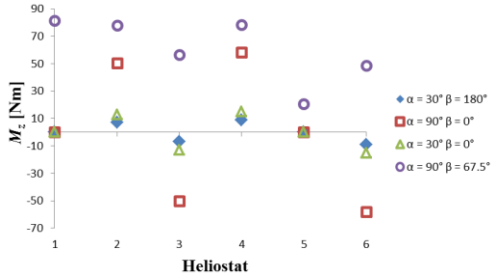

Figure 12: M_z plotted for each heliostat and orientation ($r_a = 1.5$)

Periodic repeat (Investigation 3)

The effect of continuous rows of heliostats is to partly block the flow with increasing depth into the field. This causes the second and third rows to experience reduced wind loadings as compared to the first. Figure 13 shows the flowfield for the periodically repeating geometry with a direct oncoming wind. The front heliostats can be seen blocking the flow as is evident from the lower pressures on the second and third row reflectors.

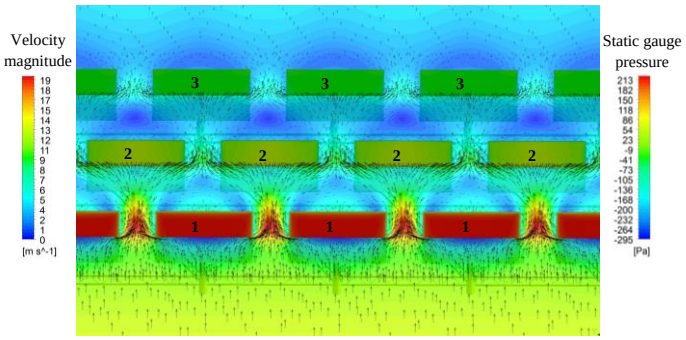

Figure 13: Velocity magnitude (horizontal plane at centre height) and static gauge pressure (reflectors) plots for the periodic case ($\alpha = 90°, \beta = 0°$)

Figure 14 shows the forces obtained per heliostat for each row and orientation (near zero values were omitted to make for a less cluttered graph). The first row of heliostats is seen to experience a larger force than was the case for a standalone unit. This is mainly due to the flow not being able to react sideways to the disturbance of the structure before encountering yet another reflector. An interesting observation is the continuous reduction in loadings at all orientations with increasing depth into the field due to blockage. Similar observations are made for the moments plotted in Figure 15.

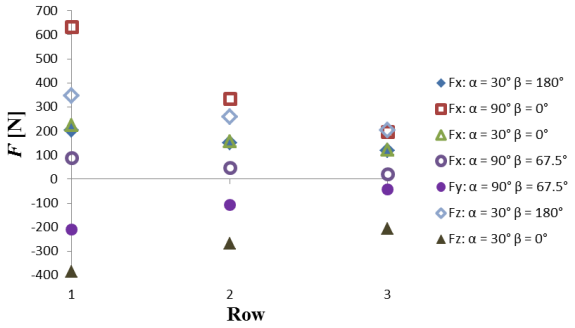

Figure 14: Forces plotted for each row and orientation ($r_a = 1.5$)

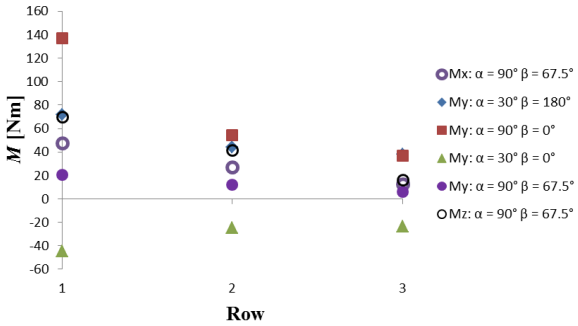

Figure 15: Moments plotted for each row and orientation ($r_a = 1.5$)

Figure 16 is a plot of the % reduction in F_x achieved for upright reflectors ($\alpha = 90°, \beta = 0°$) due to upstream rows. The results are compared to those obtained by Peterka, *et al.* [2], keeping in mind that the Peterka heliostats would stand higher in the ABL, having an elevation axis height of around 4 meters and a reflector area of 40 m^2. The amount of load reduction is also influenced by field density and it should be noted that a reflector with $r_a = 1$ would allow heliostats to be positioned closer to one another, something not considered in this study.

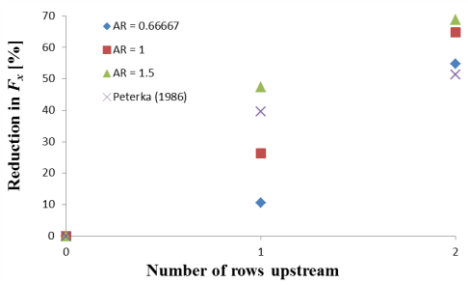

Figure 16: Reduction in F_x ($\alpha = 90°, \beta = 0°$) deeper into the field

The effects of aspect ratio

Heliostat aspect ratio has previously been shown to have an effect on wind loadings, especially moments [3]. In Figure 17 and Figure 18 the change in maximum moments brought about by a change in aspect ratio is displayed. The values plotted are the largest values obtained, regardless of orientation and represent the increase or decrease in the worst-case load. For a standalone HelioPOD, an increase in aspect ratio causes an increase in the wind-induced moment about the *z*-axis (Figure 18) and a decrease in the moment about the *y*-axis (Figure 17) for all six heliostats.

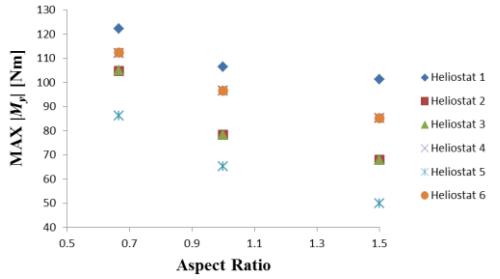

Figure 17: Variation of M_y with aspect ratio for a standalone HelioPOD

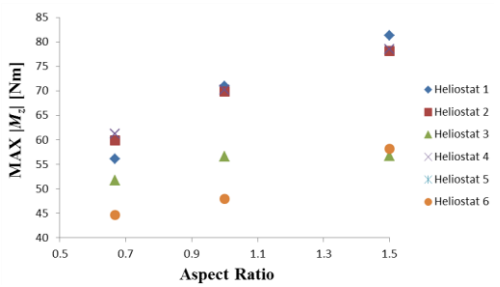

Figure 18: Variation of M_z with aspect ratio for a standalone HelioPOD

Figure 19 gives the dependency of M_z and M_y on aspect ratio for the periodically repeating case, again showing the maximum values obtained at all orientations considered. Except for the fact that M_y in the first row is rather insensitive to a change in r_a, the same observations are made than for a standalone unit.

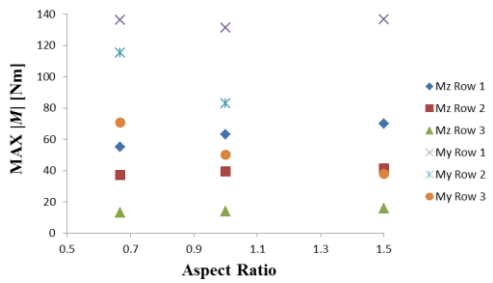

Figure 19: Variation in M_y and M_z with aspect ratio for a periodic repeat

CONCLUSION

In this investigation steady state CFD simulations were conducted to investigate the effects of wind loadings on a heliostat pod with six reflectors. In this manner mean loadings were obtained. A comparison between a standalone HelioPOD structure and continuous rows of heliostats was made. Different aspect ratios were considered and it was observed that changing the aspect ratio had an influence on the wind loadings, especially the moments. Once appropriate objective functions are determined, the aspect ratio could be optimized as in Marais, *et al.* [4].

ACKNOWLEDGEMENTS

The authors would like to acknowledge the support from the University of Pretoria (South Africa), the South African National Research Foundation (DST-NRF Solar Spoke), as well as the Solar Thermal Energy Research Group (STERG) at Stellenbosch University (South Africa).

REFERENCES

[1] Kolb, G.J., Jones, S.A., Donnelly, M.W., Gorman, D., Thomas, R., Davenport, R., and Lumia, R. *Heliostat Cost Reduction Study*, Report SAND2007-3293, Sandia, New Mexico, 2007.

[2] Peterka, J.A., Hosoya, N., Bienkiewicz, B., and Cermak, J.E. *Wind load reduction for heliostats*, Report Report SERI/STR-253-2859, Solar Energy Research Institute, Golden, Colorado, USA, 1986.

[3] Pfahl, A., Buselmeier, M., and Zaschke, M., *Wind loads on heliostats and photovoltaic trackers of various aspect ratios.* Solar Energy, 2011. **85**(9): p. 2185-2201.

[4] Marais, M.D., Craig, K.J., and Meyer, J.P. *Computational flow optimization of heliostat aspect ratio for wind direction and elevation angle*. *SolarPACES 2014*. Beijing, China: 16-19 September 2014.

[5] Wu, Z. and Wang, Z., *Numerical study of wind load on heliostat.* Progress in Computational Fluid Dynamics, an International Journal, 2008. **8**(7): p. 503-509.

[6] Larmuth, J., Malan, K., and Gauché, P. *Design and cost review of 2 m^2 heliostat prototypes*. *SASEC 2014*. Port Elizabeth, South Africa: 27-29 January 2014.

[7] Strachan, J.W. and Houser, R.M. *Testing and evaluation of large-area heliostats for solar thermal applications*, Report SAND92-1381, Sandia, New Mexico, 1993.

[8] Roos, T.H. *A wind loading correlation for an isolated square heliostat, part 1: lift and drag forces*. *SASEC 2012*. Stellenbosch, South Africa: 21-23 May 2012.

[9] Blocken, B., Stathopoulos, T., and Carmeliet, J., *CFD simulation of the atmospheric boundary layer: wall function problems.* Atmospheric environment, 2007. **41**(2): p. 238-252.